Extraction of Patient-Specific 3D Cerebral Artery and Wall Thickness Models from 2D OCT and Structured-Light 3D Scanner Data

S. Glaßer[1], T. Hoffmann[2,3], S. Voß[4], F. Klink[5], B. Preim[1]

[1] *Department of Simulation and Graphics, Otto-von-Guericke University of Magdeburg, Germany*

[2] *Department of Medical Engineering, Otto-von-Guericke University of Magdeburg, Germany*

[3] *Institute of Neuroradiology, Otto-von-Guericke University of Magdeburg, Germany*

[4]*Department of Fluid Dynamics and Technical Flows, Otto-von-Guericke University of Magdeburg, Germany*

[5] *Department of Mechanical Engineering, Otto-von-Guericke University of Magdeburg, Germany*

contact: sylvia.glasser@ovgu.de

Abstract:

We present a work flow for the virtual generation of patient-specific 3D cerebral vessel models including the vessel wall thickness. Optical coherence tomography (OCT) is employed for the acquisition of post mortem cerebral vessel image data including the cerebral vessel wall information. Due to OCT image acquisition, the 3D spatial information about the catheter's path is lost. To overcome this limitation, structured-light 3D scanning is used to obtain landmarks for the approximation of the patient-specific spatial variation of the Circle of Willis (CoW). With a geometrical transformation of the OCT image data to the extracted 3D positions, the vessel's 3D centerline can be approximated and the segmented contours are translated accordingly. We developed a 3D visualization that allows for 3D evaluation of wall thickness variations. With the presented pipeline, the surface meshes of patient-specific vessel wall models are generated which may be the prerequisite for more complex applications including fluid-structure simulations.

Key words: OCT, intracranial vessels, wall thickness, 3D orientation

1 Problem

For an improved diagnosis, therapy planning as well as clinical research, 3D surface meshes of patient-specific vessels are widely used. The evaluation of cerebral vessel pathologies like stenoses, strokes or aneurysms, mainly focuses on the vessel lumen due to the missing image modality of the vessel wall. Hence, many studies use the segmented vessel lumina for surface model generation. For example, these surface meshes allow for aneurysm evaluation based on morphological criteria like aneurysm neck size [1,2]. Further, the aneurysm's hemodynamics can be described using computational fluid dynamics simulations. This method is widely used to evaluate flow characteristic related to aneurysm rupture [3,4]. However, the vessel wall is only insufficiently included or not included at all due to the missing image modality. Our approach includes the wall thickness and creates 3D patient-specific models in order to close the gap towards more complex medical visualizations and fluid-structure simulations.

Intravascular imaging like optical coherence tomography (OCT) allows for assessment of the vessel wall and has been successfully employed in clinical practice for cardiology [5]. The co-registration of intravascular imaging to X-ray angiography allows for 3D segmentation of the intravascular image data and an extraction of the 3D centerline of the coronary artery [6] for improved diagnosis. We apply the novel application of OCT to cerebral vessels. Due to restrictions of the medical board w.r.t. catheter dimensions and stiffness of currently available systems, the in vivo imaging is not possible. However, OCT has high potential for the diagnosis of pathologies like arteriosclerotic plaque [7] as well as the rupture assessment of cerebral aneurysms [8]. Therefore, we carried out a post mortem analysis and OCT imaging of a

human Circle of Willis (CoW). With this catheter-based technique only 2D slices of the vessel cross sections are acquired, but the 3D spatial information of the vessel centerline is missing. Whereas in vivo imaging could be combined with angiographic image data yielding a 3D reconstruction of the catheter's probing path, the post mortem ex vivo imaging is not suitable for this procedure without a special application from the ethics committee. This procedure would also exceed standard forensic investigation. Therefore, we developed a setup which includes a landmark-based acquisition of the 3D spatial orientation of the CoW with structured-light scanning. Hence, the structured light scanning can be carried out during autopsy.

As a result, we can create ex-vivo patient-individual 3D OCT image data representations which allow for the examination of cerebral pathologies, manifested in the cerebral arterial wall. Our method for the extraction of a virtual 3D cerebral vessel wall thickness is explained for the carotid-anterior bifurcation.

2 Material and Methods

For the extraction of 3D information, the medical image data was analyzed and preprocessed, which is illustrated in Fig. 1. In the following, the image data acquisition and the different steps of the pipeline are explained.
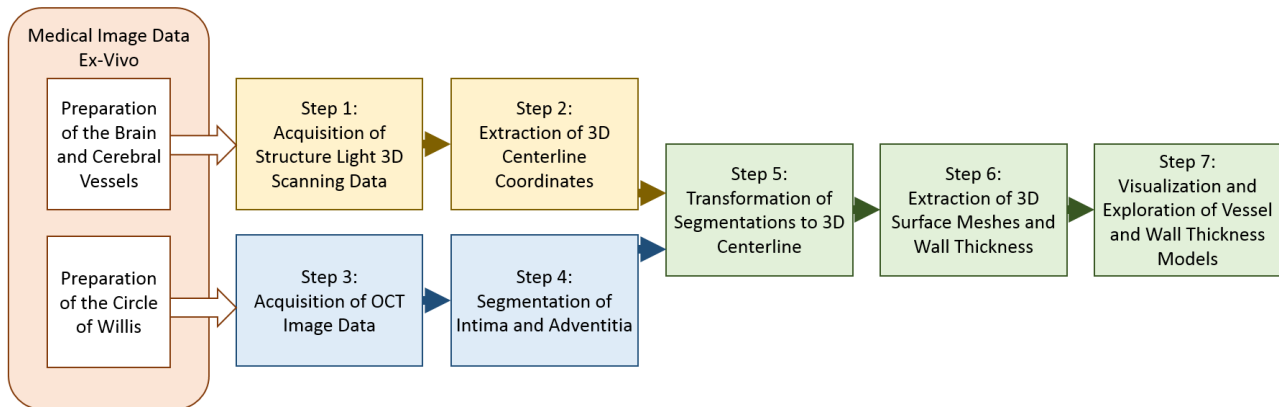

Fig. 1: Illustration of the work flow for extraction of 3D vessel wall and wall thickness models.

Medical Data

In accordance with the local ethics committee a complete CoW of a 66 year old male cadaver was explanted within a standard forensic investigation. For preparation of the specimen, the internal carotid arteries and vertebral arteries were cut proximal to the skull base and afterwards the brain was extracted. The CoW was flushed with formaldehyde (4%) to remove blood and avoid a collapse of the vessels after explantation from the brain. Hence, the 3D spatial position and orientation of the CoW were extracted with structured-light 3D scanning, which will be described in Step 1. The CoW was cut at the middle cerebral artery segment M1, in the anterior cerebral artery and posterior cerebral arteries to remove the CoW from the brain tissue. Immediately after explantation, the specimen was put into formaldehyde (4%) for fixation. The OCT imaging will be described in Step 3.

Step 1: Acquisition of Structured-Light 3D Scanning Data

For the 3D spatial orientation of the CoW, a GOM Atos Compact Scan 2M structured-light 3D scanner with a GOM touchprobe PM8 (both GOM - Gesellschaft für Optische Messtechnik mbH, Braunschweig, Germany) was used for scanning the artery surface. The system provides a measuring area of $1000 \times 750\,mm^2$ with 2 million camera pixels. Data recording and processing was done with GOM Inspect Professional (GOM - Gesellschaft für Optische Messtechnik mbH, Braunschweig, Germany).

The experimental setup is illustrated in Fig. 2. A non-reflecting black bowl was prepared with optical markers as reference objects for the calibration of the scanner coordinate system. The prepared brain was positioned upside down in the bowl to provide access to the arteries of the CoW. The position of the scanner was changed to different locations for a free field of view on the vessel of investigation. For the measurement of the 3D landmarks, the touchprobe tip was positioned on different characteristic points at the CoW. These landmarks were also used as landmarks in the OCT data sets. For the measurement of the middle cerebral artery coordinates, the temporal lobes of the brain were slightly spread to position the touchprobe tip at the vessel surface.

Step 2: Approximation of 3D Centerlines from Scanned Data

From the acquired 3D spatial positions, the centerlines of the CoW were reconstructed. Therefore, splines were fitted through the acquired image positions, recall Fig. 2C. This step was carried out in Matlab 2015b (The MathWorks, Natick, United States). A correlation of 3D positions and acquired medical image data was carried out by identification of the corresponding artery bifurcations in the OCT image data. The centerline is equidistantly sampled such that for each OCT slice the corresponding centerline point is defined.
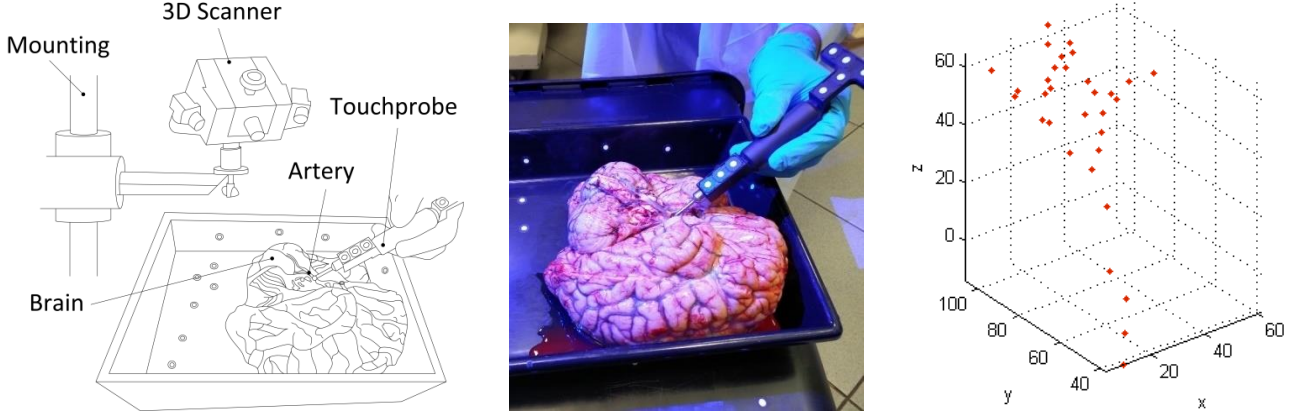

Fig. 2: Acquisition of the landmark-based spatial orientation of the CoW. A) Schematic sketch of the experimental setup. B) Depiction of the measurement. C) Extracted set of 3D positions.

Step 3: OCT Imaging

The OCT imaging was acquired with an ILUMIEN™ OPTIS™ System in combination with a 2.7F Dragonfly™ Duo OCT Imaging Catheter (both St. Jude Medical, Inc., Little Canada, Minnesota; USA) with 15 μm axial slice resolution. The specimen was placed in a box filled with saline to create an absorption behavior like in clinical scenario. Characteristic structures of the arteries were marked with steel needles (approx. 0.4 mm diameter) for recognition in the OCT image. For the measurements, the OCT catheter was carefully inserted in the vessel of investigation. A pullback of 54 mm was done three times for each artery segment. Our image data comprises the following parameters: 1024×1024 pixels image plane, 540 slices, and $9.1\ \mu m \times 9.1\ \mu m \times 0.1\ mm$ reconstructed voxel size.

Step 4: Segmentation of Vessel Walls

Segmentation of the intima and the adventitia was manually carried out in MeVisLab 2.7 (MeVis Medical Solutions AG, Bremen, Germany, www.mevislab.de). Each slice was segmented using MeVisLab's Contour Segmentation Objects library. In case of vessel bifurcations, the cross section does not show a closed vessel wall and no segmentation was carried out for this slice. To reduce the deflation of the vessel due to the ex-vivo imaging, we apply the virtual inflation method [9]. Hence, the vessel segmentations are slice-wise virtually inflated yielding a circular intima, i.e., the border between vessel lumen and wall, with a transformed adventitia, i.e., the border between wall and surrounding tissue, whereas the wall thickness for each intima point remains constant.

Step 5: Adaption of OCT Data to 3D Centerline

For the adaption of the OCT data to the 3D centerline extracted in Step 2, we transform the slices from their pixel coordinate system, given by the imaging setup, into the world coordinate system, given by Matlab and the 3D centerline, see Fig. 3. This procedure involves three stages.

In the first stage, the OCT slice is centered on the mean position of the corresponding intima segmentation, i.e., it is translated into the origin of the world coordinate system. A rotation of 90° is carried out along Matlab's x-axis and a rotation of 180° around the z-axis such that the OCT slice orientation matches the Matlab coordinate system's orientation.

The second stage is illustrated in Fig. 3A. We rotate the plane given by the current OCT slice such that its normal $\overrightarrow{v_n}$ falls onto the tangential vector $\overrightarrow{v_t}$ of the current centerline point c. The tangential vector $\overrightarrow{v_t}$ is approximated as $t = c_{i+1} - c_{i-1}$, where c_{i-1} is the predecessor and c_{i+1} is the successor of c along the centerline. Therefore, we extract the help vector $\overrightarrow{v_a}$ based on the tangential vector $\overrightarrow{v_t}$ and the up vector $\overrightarrow{v_{up}}$ of the OCT slice $\overrightarrow{v_{up}}$, with $\overrightarrow{v_{up}} = (1,0,0)^T$. We obtain $\overrightarrow{v_a} = \overrightarrow{v_n} \times \overrightarrow{v_t}$. Next, we rotate the OCT slice around the rotation axis $c + \overrightarrow{v_a}$ with angle α, where α is the angle between $\overrightarrow{v_n}$ and $\overrightarrow{v_t}$.

In the third stage, we correct the orientation of the OCT slice w.r.t. the up vector, see Fig. 4B. We extract the help vector $\vec{v_b} = \vec{v_t} \times ((1,0,0)^T \times \vec{v_t})$. We rotate the slice around the rotation axis $c + \vec{v_b}$ with the angle β, where β is the angle between $\vec{v_{up}}$ and $\vec{v_b}$. Note that $\vec{v_{up}}$ has been previously rotated and does not equal $(1,0,0)^T$ anymore. Finally, the OCT slice has been adjusted along the centerline, see Fig. 4C.
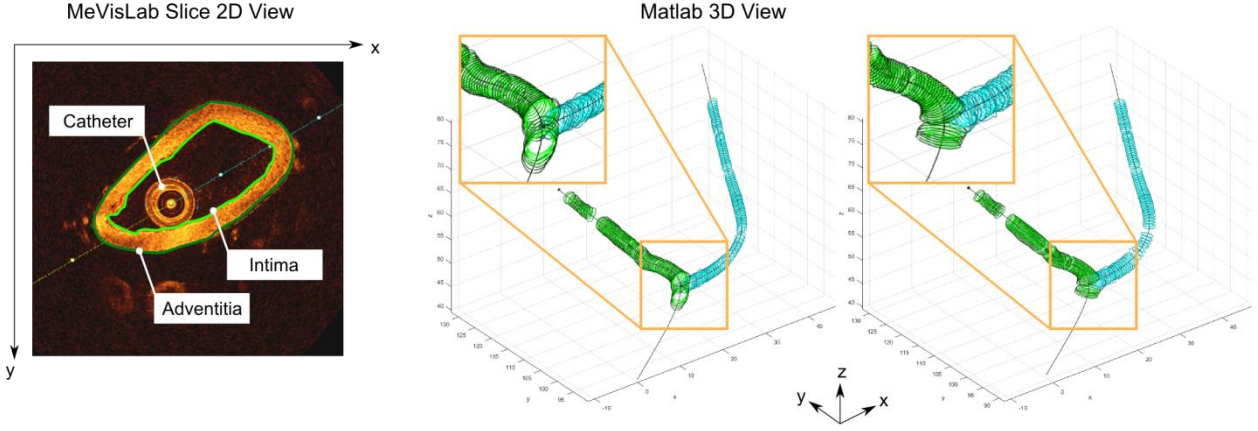

Fig. 3: Adaption of the OCT image data to the approximated 3D centerline. Left, an image slice with intima (light green) and adventitia (dark green) segmentation is shown. At the center, the contours were transformed into the 3D world coordinate system given by Matlab. Two OCT image stacks forming a bifurcation were used, the first one was mapped to green colors, the second one mapped to cyan colors. Right, the result after orientating the OCT contours along the 3D centerline is depicted.
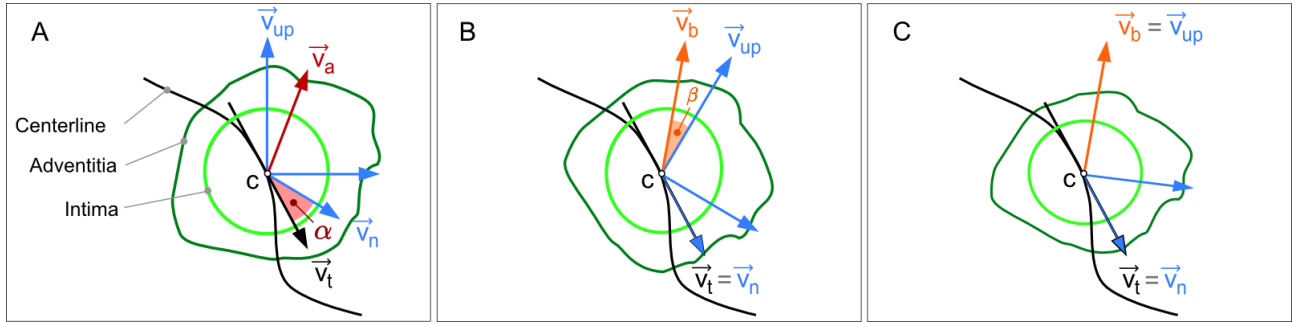

Fig. 4: Adaption of the OCT contours to the approximated 3D centerline at the centerline point c. A) First, a rotation around the help vector $\vec{v_a}$ with angle α is carried out. B) Second, a rotation around $\vec{v_t}$ with angle β is carried out, yielding the result shown in C).

Step 6: Extraction of Surface Meshes and Wall Thickness Measurement

Based on the centerline-aligned OCT slices, we carry out surface mesh extraction for the intima and the adventitia. Therefore, we equidistantly sample each intima contour in clockwise order. For the presented example, we divide each contour into 100 points. We always start at the intima point that is positioned at 12 o'clock, i.e., at the intersection of the centerline point $c + \vec{v_{up}}$ and the intima contour. Then, we construct triangle strips connecting the adjacent intima contours. We repeat this procedure for all intima contours to obtain the intima triangle surface mesh. Analogously, we extract the surface mesh for the adventitia. For both surface meshes, we carry out a triangle subdivision followed by Laplacian smoothing in Blender 2.74 (Blender Foundation, Amsterdam, the Netherlands).

For the wall thickness measurement, the distance from the intima surface to the adventitia surface has to be extracted in the direction of the intima normals. Hence, a distance approximated as nearest point between two surface meshes would not represent the wall thickness in a correct way in areas with high curvature. Therefore, the normal $\vec{n_i}$ is extracted for each vertex v_i of the intima surface mesh. It is ensured that $\vec{n_i}$ points outwards. Next, for each ray originating at v_i in direction of vector $\vec{v_i n_i}$, the intersection with all triangles from the surface mesh representing the adventitia is calculated. The distance between v_i and the intersection point yields the wall thickness for v_i.

Step 7: Combined Visualization of Surface and Wall Thickness

The visualization was implemented in MeVisLab 2.7. Based on the intima surface mesh, a color-coded surface view was generated, where the wall thickness values are mapped to color, see Fig 5. Optionally, the adventitia surface mesh could be additionally viewed as transparent edge-enhanced surface. The color-coding highlights areas with decreased wall thickness values, see Fig. 5B, as well as areas with increased wall thickness values, see Fig. 5C.
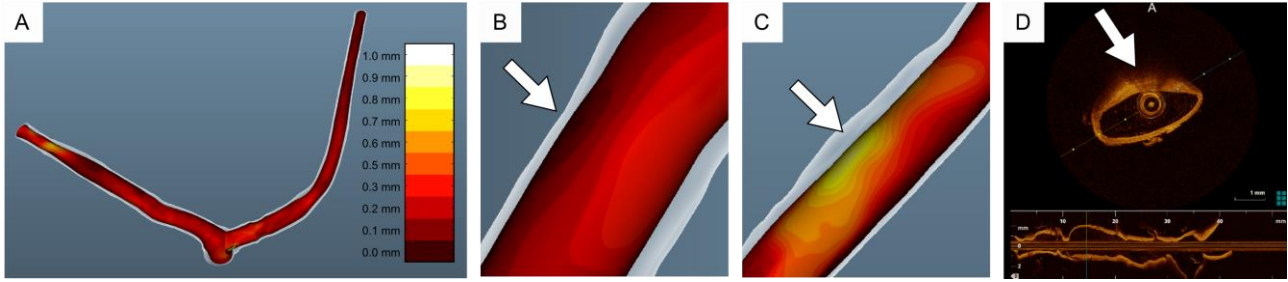
Fig. 5: Visualization of the surface meshes with color-coded extracted wall thickness value. The adventitia surface mesh can be optionally enabled or disabled. A) Example bifurcation of internal carotid artery and anterior artery. Matlab's color map "hot" (a heated body color scale, depicted in Fig. 5A) is employed to map distance from $0\ mm$ to $1\ mm$. B) Thin walls are color-coded to dark red (see arrow). C) Thicker walls are color-coded to yellow (see arrow). D) OCT view of an arteriosclerotic plaque (marked with arrow) which corresponds to the increased wall thickness in C).

3   Results

The resulting surface meshes provide novel information about the wall thickness of cerebral vessel walls acquired with OCT image data. The clinical researcher can explore the wall thickness as well as its variations in the spatial context, recall Fig. 5. Hence, the patient suffered from arteriosclerotic plaque which can be detected in the 3D view, recall Fig. 5C and Fig. 5D. Information about the quantitative distribution of wall thickness values are provided in Fig. 6. The surface meshes are the basis for subsequent analysis, like computational fluid dynamics simulation with the integration of wall thickness for the fluid-structure interaction.
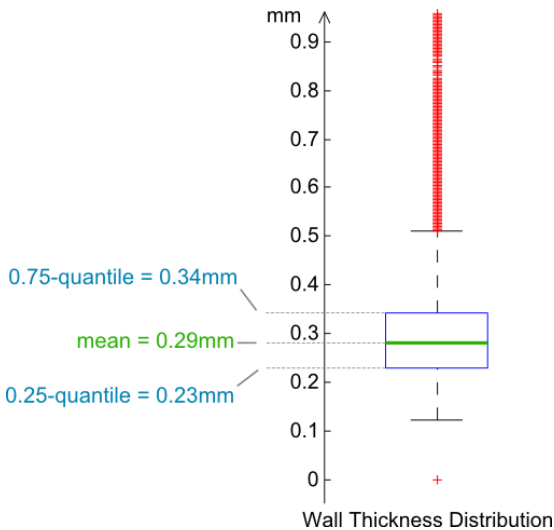

Fig. 6: Box plot of the extracted wall thickness values. A red cross indicates outliers, i.e., data values below one standard deviation above and below the mean of the data (indicated by the box plot's whiskers). The surface mesh comprises more than 75.000 vertices and the number of box plot outliers equals 271. The average wall thickness equals $0.29\ mm$.

4   Discussion

Our setup allows for a 3D reconstruction of OCT image data where the spatial information has been lost due to the ex vivo imaging. Hence, various artifacts may hamper the imaging result, e.g., shrinkage artifacts or intima detachment. Furthermore, the stiffness of the catheter may alter the natural vessel extent and shaped form. The resulting intima and adventitia surface meshes are a discrete approximation of the wall. Thus, wall thickness estimation based on normal vectors of the discrete triangle meshes could be hampered yielding the outliers presented in Section 3.

The segmentation of the vessel walls was not focus of this work. For future work, an automatic segmentation could be adapted to the described datasets, similar to [10]. Also, the mesh tessellation could be automatically carried out. The process of mapping OCT data to 3D positions based on structured-light scanning data could also be combined with other data, e.g., a centerline extracted from dyna-CT angiography data. However, the challenge of our image acquisition was caused by the ex vivo imaging. The represented surface models should be further analyzed w.r.t. computational fluid dynamics simulation and fluid-structure interaction. A quantitative comparison of the numerical results could provide information about the influence of the integration of the 3D orientation. For clinical education, a more advanced visual-

ization concept could be developed. For example, an interactive fly-through view could be provided, where MPR views along the centerline provide the OCT information, e.g., pathological changes like arteriosclerotic plaque.

5   Summary

We presented a work flow for the extraction of patient-specific 3D cerebral vessel and wall thickness models. Our work is based on the geometrical transformation of OCT image data. The resulting visualization allows for the 3D evaluation of wall thickness variations. Most important, we provide a pipeline to map OCT data for a spatial vessel reconstruction which could also be combined with other data, e.g., a centerline extracted from dyna-CT angiography data.

6   Acknowledgements

7   References

[1]   R. R. Lall, C. S. Eddleman, B. R. Bendok, H. H. Batjer, *Unruptured Intracranial Aneurysms and the Assessment of Rupture Risk Based on Anatomical and Morphological Factors: Sifting through the Sands of Data*. Neurosurgical Focus **26 (5)**, E2, (2009)

[2]   M. Neugebauer, K. Lawonn, O. Beuing, B. Preim, *Automatic Generation of Anatomic Characteristics from Cerebral Aneurysm Surface Models*. International Journal of Computer Assisted Radiology and Surgery, **8(2)**, 279-289, (2013)

[3]   P. Berg, C. Roloff, O. Beuing and et al., *The Computational Fluid Dynamics Rupture Challenge 2013—Phase II: Variability of Hemodynamic Simulations in two Intracranial Aneurysms,* Journal of Biomechanical Engineering, **137(12)**,121008, (2015)

[4]   B. Chung, J.R. Cebral, *CFD for evaluation and treatment planning of aneurysms: Review of Proposed Clinical Uses and Their Challenges*, Ann Biomed Eng **43**, 122–138, (2015)

[5]   V. D. Tsakanikas, L. K. Maichalis, D. I. Fotiadis, K. K. Naka, C. V. Bourantas: *Intravascular Imaging; Current Applications and Research Developments*. IGI Global, (2012)

[6]   S. Tu, N. R. Holm, G. Koning, Z. Huang, J. H. Reiber, *Fusion of 3D QCA and IVUS/OCT*, International Journal of Cardiovascular Imaging, **27(2)**, 197-207, (2011)

[7]   S. Yoshimura, M. Kawasaki, K. Yamada, and et al., *Visualization of Internal Carotid Artery Atherosclerotic Plaques in Symptomatic and Asymptomatic Patients: A Comparison of Optical Coherence Tomography and Intravascular Ultrasound*, American Journal of Neuroradiology, **33(2)**, 308–313, (2012)

[8]   T. Hoffmann, S. Glaßer, A. Boese, and et al., *Experimental Investigation of Intravascular OCT for Imaging of Intracranial Aneurysms*. International Journal of Computer Assisted Radiology and Surgery, **11(2)**, pp. 231-41, (2016)

[9]   S. Glaßer, T. Hoffmann, A. Boese, S. Voß et al., *Histology-Based Evaluation of Optical Coherence Tomographic Characteristics of the Cerebral Artery Wall via Virtual Inflating*, Proc. of Eurographics Workshop on Visual Computing in Biology and Medicine, Chester UK, pp. 149-158 (2015)

[10]   K.-P. Tung, W.-Z. Shi, R. DeSilva, E. Edwards, D. Rueckert, *Automatical Vessel Wall Detection in Intravascular Coronary OCT*, Proc. of IEEE Symp. On Biomedical Imaging: From Nano to Macro, 610-613, (2011)